CDF note 10978

Search for Rare Z Decays into Two Reconstructed Photons at CDF

The CDF Collaboration
URL http://www-cdf.fnal.gov
(Dated: March 9, 2013)

We report the most sensitive search to date for forbidden and exotic decays of the Z boson to a pair of photons, a pair of neutral mesons, or a neutral meson and a photon. The search is using the full CDF dataset corresponding to 10.0 fb^{-1} of integrated luminosity. The two decay products are reconstructed in the electromagnetic calorimeter, spanning a rapidity range of $|\eta| < 1.1$, and their momenta are used to reconstruct the invariant mass of the pair that is used to identify Z bosons. Bayesian 95% C.L. limits on the signal branching ratio are derived by fitting the signal and background expectations to the data in the Z-mass window of [80,102] GeV/c^2, using a binned likelihood based on the mass distribution. The observed branching ratio limits presented here are 1.66×10^{-5} for $Z\to\gamma\gamma$, 2.28×10^{-5} for $Z\to\pi^0\gamma$, and 1.73×10^{-5} for $Z\to\pi^0\pi^0$. The $Z\to\gamma\gamma$ and $Z\to\pi^0\gamma$ limits are more sensitive by factors of 3.1 and 2.3, respectively, than the most stringent Particle Data Group limits reported by experiments at the LEP collider. The $Z\to\pi^0\pi^0$ branching ratio limit is the first limit reported in this decay mode.

Preliminary Results for Winter 2013 Conferences

I. INTRODUCTION

In principle, the $Z\to\gamma\gamma$ decay could be considered as an extension of the non-abelian structure of the weak interaction into the electromagnetic sector through a trilinear boson coupling. The Landau-Yang theorem [1, 2] forbids this decay, however. The question is whether an indirect interaction mechanism, such as a higher-order excitation of standard model fermion fields or an extraneous mediator field, can change the arguments of the theorem and allow the decay at a relatively low rate. The search for this decay mode then becomes a test of higher-order corrections to the electroweak interaction, also probing possible new physics. On the theory side, a recent calculation [3], based on fermion loop corrections to the electroweak interaction, provided expectations for the decay branching fraction of $\mathcal{O}(10^{-8})$. This order of magnitude is heuristically justified on $\mathcal{O}(\alpha^{-4})$ grounds for two photon production by fermions. On the experimental side, limits are reported [4] on the branching ratios of both the $Z\to\gamma\gamma$ decay mode as well as the $Z\to\pi^0\gamma$ mode. The latter is quantum-mechanically allowed and can serve as a gauge of higher-order corrections by computing its expected rate with the aid of an effective quark-pion coupling associated with quark-photon and quark-Z vertices [5, 6]. In that case, the effective quark-pion interaction suppresses further the branching fraction, down to $\mathcal{O}(10^{-10})$. The most stringent existing experimental limits on $Z\to\gamma\gamma$ and $Z\to\pi^0\gamma$ branching ratios come from the LEP experiment [7] and are of $\mathcal{O}(10^{-5})$. Specifically, they set a limit of 5.2×10^{-5} on the branching ratio of both decay modes. The LEP experiment did not measure a limit on the $\pi^0\pi^0$ decay mode.

In Z decays involving a π^0, the neutral pion is isolated (not contained in a jet) and decays about 99% of the time into a pair of photons. Because of the high momentum of the π^0 from a Z decay, the photon pair is collinear, usually producing a sufficiently narrow angle such that the two photons appear in the central shower-maximum (CES) detector and the central electromagnetic (CEM) calorimeter as a single electromagnetic (EM) shower. The result is that the π^0 has nearly the same signature as an isolated photon, with only a slightly smaller central photon identification efficiency.

With such low branching ratio expectations of the signals, the experimental search for $Z\to\gamma\gamma$, $Z\to\pi^0\gamma$, and $Z\to\pi^0\pi^0$ decays is challenging. However, with the abundance of Z bosons produced in high-energy hadron colliders, such as the Tevatron and the LHC, and the good understanding of the backgrounds in those environments, it is possible to improve the existing LEP limits by a significant factor. The intensive effort for the search of the standard model Higgs boson in the diphoton decay mode at both environments has developed analysis tools that can be directly applied in the $Z\to\gamma\gamma$, $Z\to\pi^0\gamma$, and $Z\to\pi^0\pi^0$ searches. No limits from either the Tevatron or the LHC on the branching ratios of those decay modes have been reported so far. The present work is a search for those modes using the full CDF dataset.

II. DATA SAMPLE & EVENT SELECTION

We use the same diphoton event selection that has recently been used in the published SM $H\to\gamma\gamma$ analysis [8–10], with the only difference that we focus only on events in which there are two central ($|\eta|<1.1$) photons. We use data corresponding to 10.0 fb^{-1} of integrated luminosity, taken between February 2004 and September 2011. Diphoton data events are collected with a single photon trigger (Table I), where the trigger efficiency for events that pass the full CC diphoton selection is found to be 99.8%. This trigger efficiency is determined by Monte Carlo (MC) simulation [8–10] and is included when normalizing all MC samples. The efficiency is validated in $Z\to e^+e^-$ decays in both data and MC, from which an uncertainty of 1% is derived [8–10].

Level 1	E_T ($z=0$)	>8.0
Level 2	E_T ($z=0$)	>21.0
	Had/Em	<0.125
	Calorimeter Isolation	<3.0 || $<0.15E_T$
Level 3	E_T ($z=0$)	>25.0
	CES χ^2	<20
	Had/Em	$<0.055+0.00045\times E$ ($E<200$ GeV)
		$<0.2+0.001\times E$ ($E>200$ GeV)
	Calorimeter Isolation	$<0.10E_T$

TABLE I: Photon trigger requirements.

The z position of the event vertex must be within 60 cm of zero. The overall efficiency for this cut is $(97.43\pm0.07)\%$. This efficiency and its corresponding uncertainty are applied to the normalization of all MC samples. Of the events that pass the previous selection, we next search for the two highest E_T photon candidates that pass the tight central

photon identification requirements described in Section II A. We then define the signal region by selecting events for which the diphoton mass $m_{\gamma\gamma}$ is in the region 91 ± 11 GeV/c^2, which contains about 90% of the signal. The sideband control region is defined by $m_{\gamma\gamma}$ values that are outside of the signal region. The full diphoton selection is inclusive, which means we search for two photons, but other objects (including more photons) may also be in the event.

A. Photon Identification

In order to identify central, isolated EM showers with no associated tracks, we apply a neural network (NN) photon selection. This is described in detail in References [8–10], and is summarized briefly here. A list of the cuts is provided in Table II.

Central Photon Variable	Cut
E_T	> 15 GeV
CES Fiducial	$\lvert x_{\rm CES}\rvert < 21$ cm, $9 < \lvert z_{\rm CES}\rvert < 230$ cm
Had/Em	< 0.125
Calorimeter Isolation	$< 0.15 E_T$ GeV for $E_T \leq 20$ GeV
	$< 3.0 + 0.02(E_T - 20.0)$ GeV for $E_T > 20$ GeV
Track Isolation	< 5 GeV/c
2nd CES Cluster E_T	$< 0.14 E_T$ GeV for $E_T < 18$ GeV
	$< 2.4 + 0.01 E_T$ GeV for $E_T > 18$ GeV
N track (N3D)	≤ 1
Track p_T (if N3D = 1)	$< 1.0 + 0.005 E_T$ GeV/c
NN Output	> 0.74

TABLE II: Central NN photon selection cuts listed in the order that they are applied.

The efficiency of the NN selection is calculated using $Z\to e^+e^-$ events in both data and MC, as a function of the number of vertices in the event. The resulting efficiency values [10] are then folded into the N_{vtx} (number of reconstructed vertices) distribution of the diphoton data and signal MC in order to obtain average data and MC efficiencies. The ratio of the average data to MC efficiency gives a scale factor of 94.4%, which is applied twice (once per photon and/or for the isolated π^0) to correct the diphoton efficiency obtained directly from the signal MC. Systematic uncertainties applied to this correction are due to detector material, photon vs electron identification, run dependence, and data/MC fits to the Z peak, giving an overall net uncertainty of $\sim$2% per photon.

III. SIGNAL MODEL

We use MC simulation to predict the diphoton mass shape and the detector acceptance $\times$ efficiency of the diphoton signal. Since PYTHIA does not model $Z\to\gamma\gamma$ decays, we start from a $Z\to\nu_e\bar{\nu}_e$ PYTHIA sample, and then convert the neutrinos to photons before showering in PYTHIA and passing through the detector and trigger simulation. We refer to the corresponding MC sample as the "unweighted $Z\to\gamma\gamma$ sample." This sample is generated using PYTHIA version 6.2.16 [11] with the CTEQ5L [12] PDF set and the standard CDF "underlying event" (UE) tune [13]. The sample has an angular distribution characteristic of the neutrino-antineutrino pair from $Z\to\nu_e\bar{\nu}_e$ decays.

A. $Z\to\gamma\gamma$ Angle-Reweighting

The detector acceptance of the photons from the $Z\to\gamma\gamma$ decay depends on their angular distribution. To obtain an appropriate model of the $Z\to\gamma\gamma$ signal, we reweight the $Z\to\gamma\gamma$ sample on an event-by-event basis using weights determined from the ratio of the expected angle of the outgoing photons to that for the outgoing neutrinos. The particular angle α used is the angle made by the γ or ν particle direction and the polar axis in the rest frame of the Z boson. The resulting weight function has the form $w(\alpha) \propto \frac{a-\cos^2\alpha}{b+\cos^2\alpha}$, where the numerator is the expected angular distribution for the photons, the denominator is the expected angular distribution for the neutrinos, and a and b are constants. The calculation of the expected $\gamma\gamma$ and $\nu\bar{\nu}$ angular distributions is described in detail in Appendix A. This procedure transforms the unweighted sample to the expected angular distribution for photons from $Z\to\gamma\gamma$ decays. We call the resulting angular-weighted sample the "weighted $Z\to\gamma\gamma$ sample" or simply the "$Z\to\gamma\gamma$ sample."

B. $Z\to\pi^0\gamma$ Photon Identfication Efficiency-Reweighting

As described in Appendix A, the π^0 and γ from the $Z\to\pi^0\gamma$ decay are expected to have the same angular distribution as the neutrinos from the $Z\to\nu_e\bar{\nu}_e$ decay; we therefore begin with the unweighted $Z\to\gamma\gamma$ sample, but apply no angle-weights. This unweighted sample has the angular distribution that we expect for the $Z\to\pi^0\gamma$ decay products, but has a diphoton efficiency that we would expect for two isolated photons. The isolated neutral pion that decays to two collinear photons is expected to have a slightly lower photon identification efficiency than a single isolated photon in the kinematic region allowed from a Z decay. An appropriate model of the $Z\to\pi^0\gamma$ decay is then obtained by reweighting the unweighted $Z\to\gamma\gamma$ sample event-by-event, based on the difference between the π^0 and γ photon identification efficiencies.

We study the difference in the π^0 and γ efficiencies to the NN photon selection using MC samples generated with a "particle gun" event generator. The particle gun produces particles with a flat E_T spectrum through 250 GeV; it does not include underlying event. From this MC sample, we determine the net photon identification efficiency as a function of generator-level E_T, obtained for both isolated photons and neutral pions. The π^0 to γ efficiency weights are then derived from their ratio. The weights are applied on an event-by-event basis, as a function of generator-level E_T. They weight the unweighted $Z\to\gamma\gamma$ sample to the efficiency expected for one isolated photon and one isolated neutral pion that decays into a collinear photon pair. The resulting efficiency-weighted sample is referred to as the "$Z\to\pi^0\gamma$ sample."

The π^0/γ efficiency weights result in a small decrease of 2% in the diphoton acceptance $\times$ efficiency relative to assuming two isolated photons from the Z decay. This small decrease is expected because the signal has E_T values near 45 GeV, in a region where the π^0/γ efficiency weights are slightly less than unity on average. We take 100% of the efficiency correction as an uncertainty on the method and therefore apply a 2% uncertainty on the π^0/γ efficiency weighting.

C. $Z\to\pi^0\pi^0$ Photon ID Efficiency-Reweighting

The $Z\to\pi^0\pi^0$ decay mode is expected to have the same angular distribution as the $Z\to\gamma\gamma$ decay. This is because identical particles exist in the final state and therefore the only option for their helicity difference is zero (see Appendix A). We, therefore, start with the angle-weighted $Z\to\gamma\gamma$ sample and then apply the π^0/γ efficiency correction of 2% from the previous section twice, once for each π^0. The $Z\to\pi^0\pi^0$ acceptance times efficiency will then be 96% smaller than that for the $Z\to\gamma\gamma$ decay. As the $Z\to\pi^0\gamma$ sample has a 2% uncertainty on this efficiency reweighting for a single π^0, we apply a systematic uncertainty of 4% for the $Z\to\pi^0\pi^0$ normalization.

D. N_{vtx} Reweighting

In addition to the angle or efficiency weights used to obtain the signal MC samples, we weight each MC sample to to the $N_{\rm vtx}$ distribution of the data, where $N_{\rm vtx}$ is the number of reconstructed vertices in an event. The mass resolution of the signal can be sensitive to this distribution, so the $N_{\rm vtx}$ reweighting provides a better representation of the signal mass shape for the current data sample.

E. Signal $m_{\gamma\gamma}$ Shape

After obtaining MC samples for each signal, we compare the resulting mass shapes. The shapes are essentially identical and we therefore assume the same $m_{\gamma\gamma}$ shape for each signal — when setting limits on the signal branching ratios, we use the single shape given in Figure 1 in the region $80 < m_{\gamma\gamma} < 102$ GeV/c^2.

F. Signal Acceptance $\times$ Efficiency

Once the $Z\to\gamma\gamma$, $Z\to\pi^0\gamma$, and $Z\to\pi^0\pi^0$ MC samples are prepared as described in previous sections, the signal acceptance $\times$ diphoton selection efficiency ($A\epsilon$) in the $m_{\gamma\gamma}$ signal region is obtained from

$$A\epsilon = (A\epsilon)_{MC} \times ({\rm SF}_\gamma)^2 \times \epsilon_{\rm vtx} \times \epsilon_{\rm trig}. \quad (1)$$

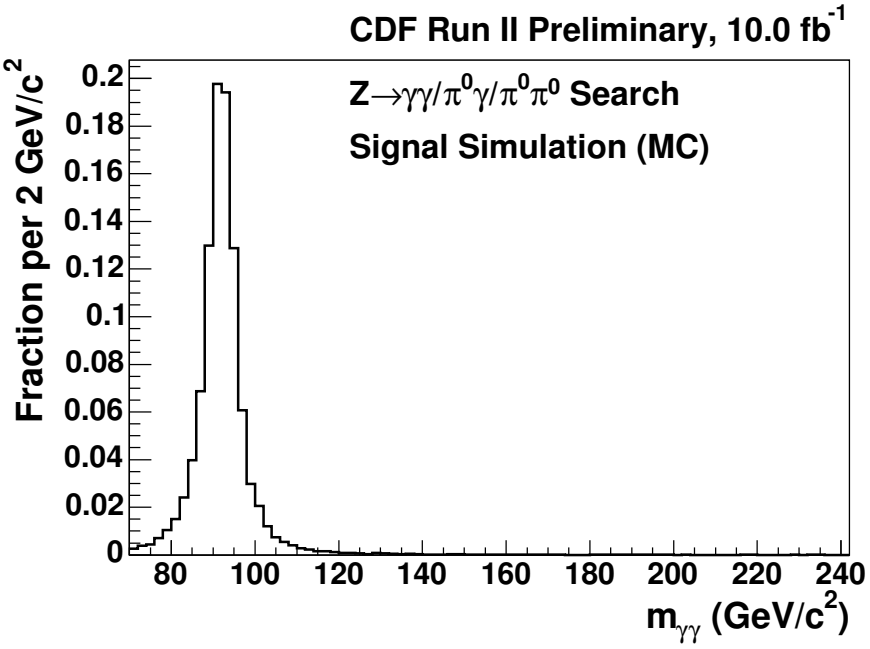

FIG. 1: Invariant diphoton mass shape assumed for the both Z→$\gamma\gamma$ and Z→$\pi^0\gamma$ signal decays. The region $80 < m_{\gamma\gamma} < 102$ GeV/c^2 is used when setting limits on the signal branching ratios.

- The $(A\epsilon)_{MC}$ term is the signal acceptance × diphoton efficiency as obtained from the signal MC. It is calculated by taking the ratio of the number of events that pass the full CC diphoton selection to the number of events that pass the $z_{\rm vtx}$ cut. For events in the $m_{\gamma\gamma}$ signal region, this $(A\epsilon)_{MC}$ value is found to be 8.9% for the Z→$\gamma\gamma$ sample, 6.4% for the Z→$\pi^0\gamma$ sample, and 8.5% for the Z→$\pi^0\pi^0$.
- The SF_γ term refers to the data-MC scale factor correction of 94.4% made to the MC photon identification efficiency. This correction was described in Section II A and is applied twice to correct the photon and/or neutral pion efficiency to the data.
- As previously mentioned, the $z_{\rm vtx}$ and trigger efficiencies ($\epsilon_{\rm vtx}$ and $\epsilon_{\rm trig}$) are taken to be 97.4% and 99.8%, respectively.

Applying these values to the Z→$\gamma\gamma$, Z→$\pi^0\gamma$, and Z→$\pi^0\pi^0$ samples in the $m_{\gamma\gamma}$ signal region gives a total $A\epsilon$ value of 7.6%, 5.5%, and 7.3%, respectively.

G. Expected Signal Yield

In principle, the expected number of Z→$\gamma\gamma$, Z→$\pi^0\gamma$, Z→$\pi^0\pi^0$ signal events could then, respectively, be obtained from

$$N_{\mathrm{Z}\to\gamma\gamma} = \frac{\sigma(Z\to ee)}{\mathrm{Br}(Z\to ee)}\cdot \mathrm{Br}(Z\to\gamma\gamma)\cdot L\cdot (A\epsilon)_{Z\to\gamma\gamma}, \tag{2}$$

$$N_{\mathrm{Z}\to\pi^0\gamma} = \frac{\sigma(Z\to ee)}{\mathrm{Br}(Z\to ee)}\cdot \mathrm{Br}(Z\to\pi^0\gamma)\cdot L\cdot (A\epsilon)_{Z\to\pi^0\gamma}, \tag{3}$$

or

$$N_{\mathrm{Z}\to\pi^0\pi^0} = \frac{\sigma(Z\to ee)}{\mathrm{Br}(Z\to ee)}\cdot \mathrm{Br}(Z\to\pi^0\pi^0)\cdot L\cdot (A\epsilon)_{Z\to\pi^0\pi^0}, \tag{4}$$

where $\sigma(Z\to ee) = 250$ pb is the Z→e^+e^- cross section, Br(Z→ee) = 0.034 is the Z→e^+e^- branching ratio, $L = 10.0$ fb^{-1} is the integrated luminosity of the data sample, and $A\epsilon$ is the acceptance × efficiency value of the

previous section. Because we make no assumption on the theoretical signal branching ratios, however, we do not calculate an expected number of signal events based on the SM theory. Section VI will instead discuss the calculation of the limit on these branching ratios from CDF data. With limits on the branching ratios, we can then produce limits on the number of signal events excluded by the data using the above equation.

H. Systematic Uncertainties on Signal Rate

An uncertainty of 6% is applied to the $Z\to e^+e^-$ cross section, taken from Reference [14]. The $Z\to\pi^0\gamma$ ($Z\to\pi^0\pi^0$) signal is given a 2% (4%) uncertainty on the π^0/γ efficiency weighting as described in Section III C. Because we use an identical event selection as the $H\to\gamma\gamma$ analysis, for the remaining uncertainties on the signal we assign the same systematic uncertainties as was done in the $H\to\gamma\gamma$ analysis. Some of these values were obtained from studies using $H\to\gamma\gamma$ MC samples, but are expected to apply to the $Z\to\gamma\gamma$ and $Z\to\pi^0\gamma$ signals as well. A brief summary of each uncertainty is provided here.

The uncertainty on the integrated luminosity is 6%. The PDF uncertainty of 5% on the event acceptance was calculated using the CTEQ61.M [15, 16] error sets and a standard event re-weighting technique [17, 18]. An intial-/final-state radiation (ISR/FSR) uncertainty of 3% was obtained by using the standard method of MC samples with modified parton shower parameters. The energy scale systematic uncertainty of the CEM calorimeter was studied by checking the effect on the acceptance of varying the CEM scale by 1%. A trigger efficiency uncertainty of 1% is described in Reference [10]. The uncertainty in the $z_{\rm vtx}$ cut is 0.2%. The uncertainty in the photon identification efficiency was discussed briefly in Section II A and is described in more detail in References [8–10].

IV. BACKGROUND MODEL

Backgrounds consist of a resonant, Drell-Yan (DY) component (about 2%) and a non-resonant component (about 98%). The modeling of each is discussed here.

A. Resonant Background (Drell-Yan)

Inclusive $Z\to e^+e^-$ MC is used to model the DY background component (Figure 2), where a pair of electrons fakes a pair of photons. We reweight this MC to the N_{vtx} distribution of the data.

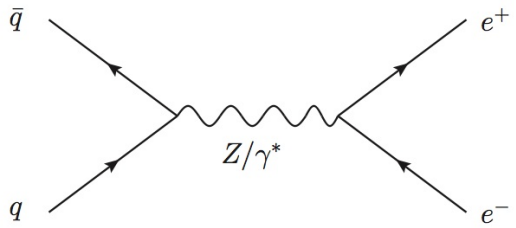

FIG. 2: Diagram of the Drell-Yan process, $q\bar{q}\to Z/\gamma^*\to e^+e^-$.

We first model this background for the whole mass range above 30 GeV/c^2, since it will be subtracted from the data before modeling the non-resonant background (described in the next section). The samples assume an inclusive cross section of 355 pb with a k-factor of 1.4, for invariant masses above 30 GeV/c^2. This cross section does not account only for the invariant mass region around the Z pole, but also for the off-shell Z events in the low invariant mass region.

To determine the expected number of events for the full $m_{\gamma\gamma}$ region, we first calculate the the acceptance × efficiency for events faking a photon pair. For $m_{\gamma\gamma}>30$ GeV/c^2, it is found that 2269 MC events pass the full diphoton selection out of 70,981,106 MC events that pass the z_{vtx} selection. We then multiply this fraction by $\epsilon_{\rm vtx}\times\epsilon_{\rm trig}=0.974\times0.998$ to get a total $A\epsilon$ for the DY component of 0.0031% for the full mass region. With 10 fb^{-1} of integrated luminosity, this gives a DY background yield of 355 pb $\cdot\,1.4\cdot 10000$ pb$^{-1}\cdot 0.000031=154$ events in the $m_{\gamma\gamma}>30$ GeV/c^2 region.

Figure 3 shows the diphoton mass shape for $m_{\gamma\gamma}>70$ GeV/c^2, which is obtained from MC events that pass the full diphoton selection (pairs of electrons faking pairs of photons). This shape is scaled to the expected number

of events for our data sample. The scaled shape is subtracted from the data before the sideband fit described in Section IV B. To determine the DY background in the signal region, we consider only the 11 bins of Figure 3 for which $80 < m_{\gamma\gamma} < 102$ GeV/c^2. Since the histogram of Figure 3 is normalized to the expected prediction, these 11 bins give the DY prediction in the signal region: 54 events.

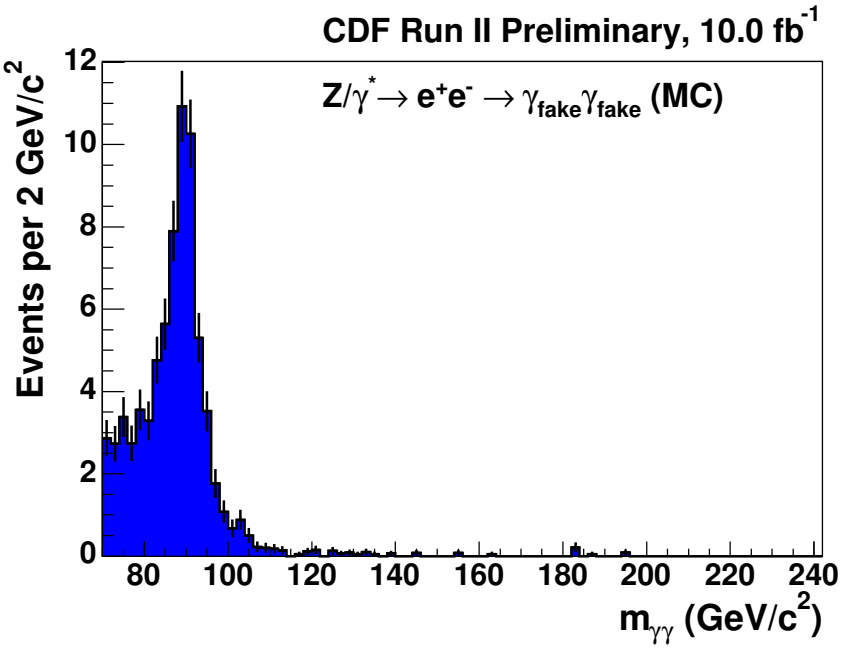

FIG. 3: The invariant diphoton mass shape of Drell-Yan MC events that fake a photon pair. The shape is scaled to the expected number of events for our data sample (154 events) as described in the text.

The dominant uncertainties on this normalization are from the luminosity (6%) and the Z cross section (6%). We also assign uncertainties on the trigger efficiency, $z_{\rm vtx}$ efficiency, and electron fake rate. The first two of these are the same uncertainties that are applied to the signal. The latter is found to be about 2%. In addition to these systematic uncertainties, we furthermore include bin-by-bin statistical uncertainties. Because the signal is dominated by the non-resonant background, it is found that the uncertainty on the DY normalization has a negligible effect on the expected sensitivity of the final branching ratio limits. We then consider any other sources of uncertainty to be negligible.

B. Non-Resonant Backgrounds ($\gamma\gamma$, γj, and jj)

The non-resonant background is the dominant background, comprising about 98% of the total background. It is composed of prompt diphoton events ($\gamma\gamma$) from QCD interactions and events in which one or two jets fake a photon (γj and jj, respectively). Figure 4 shows example leading order diagrams for these processes. The prompt diphoton background is known to comprise roughly 2/3 of the non-resonant background, while the γj and jj events comprises roughly 1/3 of the non-resonant background.

The technique for modeling the non-resonant background is similar to that used by the H→$\gamma\gamma$ analysis, where a fit is made to the sideband (control) region if the diphoton mass spectrum. The resulting fit is then used to interpolate the shape and rate of this background into the signal region. The difference with this analysis compared to the H→$\gamma\gamma$ analysis is that we first subtract the DY component from the data. We then fit to the DY-subtracted data, which is shown in Figure 5 along with the corresponding residual plot of (data – fit)/(statistical error). The resulting background yield in the $m_{\gamma\gamma} = 91 \pm 11$ GeV/c^2 signal region is 2251 events.

Background uncertainties based on the parameters of the fit function are determined, as with the H→$\gamma\gamma$ analysis, by fluctuating the parameters of the fit function for numerous trials and retaining the largest fluctuations of the predicted background yields relative to those obtained from the central fit [8–10]. The result of this procedure is a 1.8% uncertainty on the non-resonant background rate. We furthermore apply a 2% uncertainty derived from choice of the $m_{\gamma\gamma}$ fit region. Because this background comprises the majority of the total background, its total rate uncertainty is the dominant uncertainty in the analysis.

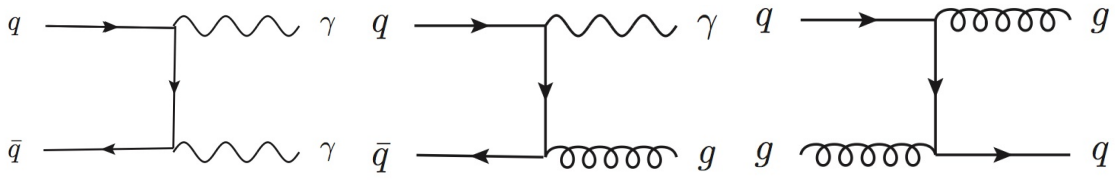

FIG. 4: Example leading order diagrams of (a) prompt diphoton production (b) γ+ jet, and (c) dijet production at hadron colliders.

V. SUMMARY OF SYSTEMATIC UNCERTAINTIES

Table III summarizes systematic uncertainties considered in the analysis. These are used in the branching ratio limit calculations described in the next section.

CDF Run II Preliminary						$\int \mathcal{L} = 10.0$ fb^{-1}
		Signal			Background	
Systematic Uncertainties (%)		$Z \to \gamma\gamma$	$Z \to \pi^0\gamma$	$Z \to \pi^0\pi^0$	Drell-Yan	Non-Resonant
Luminosity	6	✓	✓	✓	✓	
Z Cross Section	6	✓	✓	✓	✓	
PDF	5	✓	✓	✓		
ISR/FSR	3	✓	✓	✓		
Energy Scale	0.2	✓	✓	✓		
Trigger Efficiency	1	✓	✓	✓	✓	
z-Vertex	0.2	✓	✓	✓	✓	
Photon ID Efficiency	4	✓	✓	✓		
π^0/γ Efficiency	2 per π^0		✓	✓		
Electron Fake Rate	2				✓	
Sideband Fit	2.7					✓

TABLE III: Summary of the systematic errors included in the analysis.

VI. RESULTS

Figure 6 shows the DY and non-resonant backgrounds along with the data for (a) a $m_{\gamma\gamma}$ region that includes both the signal region and the sideband near the signal region and (b) a $m_{\gamma\gamma}$ region that includes only the signal region. The background and data yields in the signal region are provided in Table IV.

$Z \to \gamma\gamma/\pi^0\gamma/\pi^0\pi^0$ Search	CDF Run II Preliminary, 10.0 fb^{-1}
Process	Number of Events for $80 < m_{\gamma\gamma} < 102$ GeV
Drell-Yan	54 ± 5
$\gamma\gamma$, γj, and jj	2251 ± 61
Total background	2305 ± 61
Data	2294

TABLE IV: Event yields in the signal region ($80 < m_{\gamma\gamma} < 102$ GeV)

No excess is observed in the data and upper limits are set on the Z→$\gamma\gamma$, Z→$\pi^0\gamma$, and Z→$\pi^0\pi^0$ branching ratios. Because the signature of each signal in the CDF detector is nearly indistinguishable, we set a limit on the branching ratio of each signal by itself, assuming the other signal decay modes are not present. We calculate a Bayesian C.L. limit based on a Poisson binned likelihood constructed from each bin in the signal region (2 GeV/c^2 bin width) of the background, data, and signal mass distributions. The background and data inputs were provided in Figure 6.

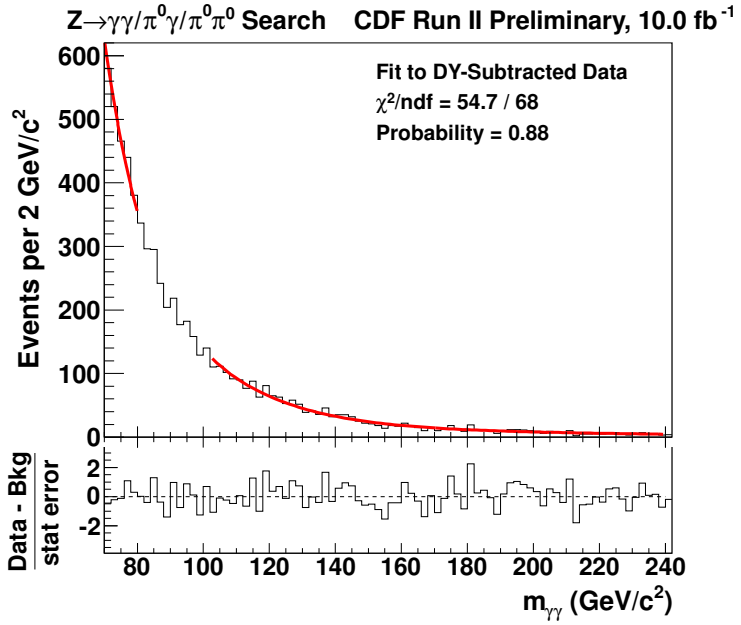

(a)

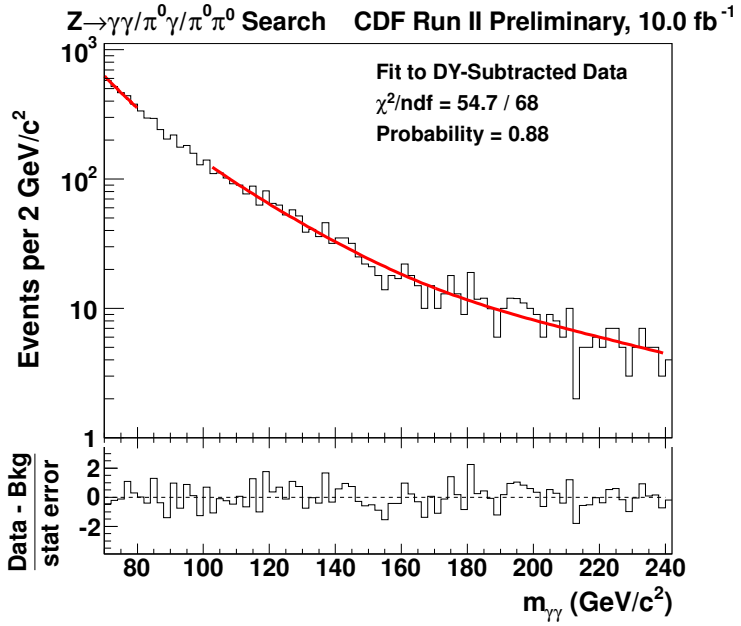

(b)

FIG. 5: The upper distribution shows a smooth fit to the $m_{\gamma\gamma}$ distribution in the DY-subtracted data. The 22 GeV/c^2 gap in the fit, centered at 91 GeV/c^2, represents the signal region that was excluded from the fit. The fit is interpolated into the signal region, which serves as the prediction of the non-resonant background in this region. The residual for the shape in the signal region is shown in the lower plot.

We normalize the signal mass shapes (Figure 1) as given by Equations 2–4, except for the signal branching ratio term, which is a parameter of the limit calculation. We assume a positive flat prior in the signal branching ratios and integrate over the Gaussian priors for the systematic uncertainties. A 95% C.L. limit is determined such that 95% of the posterior density for the branching ratio falls below the limit [4]. The observed 95% C.L. on the branching ratio is calculated from a posterior density obtained from the data.

For comparison, thousands of simulated experiments are used to calculate a set of expected 95% C.L. limits that are calculated without data, based on expected backgrounds only. The median of these simulated pseudoexperiments

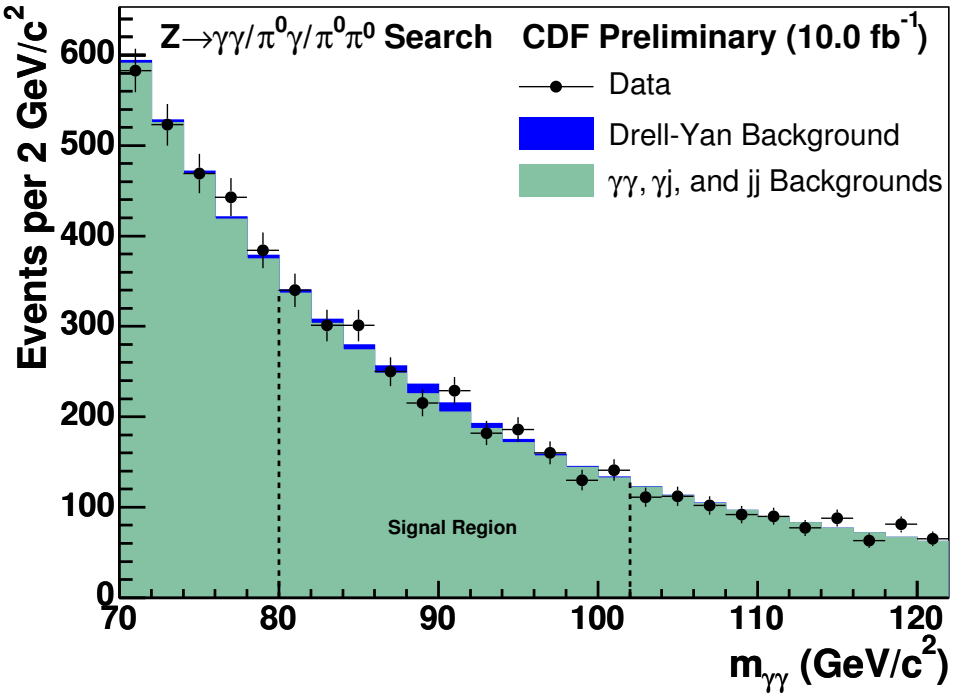

(a) Sideband plus signal region.

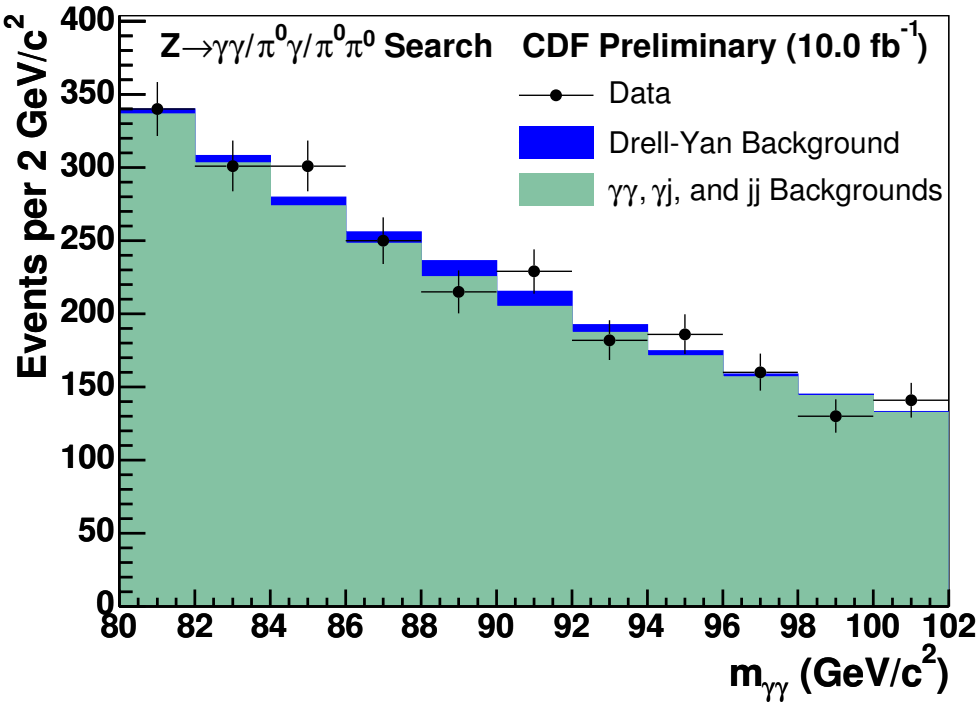

(b) Signal region.

FIG. 6: The DY and non-resonant backgrounds compared to the data for (a) the sideband plus signal region and (b) the signal region only.

is referred to as the expected limit. The region where 68% of these pseudoexperiments lie around the median is the 1σ expected region, and the region where 95% of them lie around the median is the 2σ expected region. Table V provides the expected and observed 95% C.L. limits on the $Z\to\gamma\gamma$, $Z\to\pi^0\gamma$ and $Z\to\pi^0\pi^0$ branching ratios. Again, these limits are calculated for each signal by itself, assuming the other signal is not present. The previous most

CDF Run II Preliminary						$\int \mathcal{L} = 10.0$ fb^{-1}
	95% C.L. Limits					
Signal	Expected ($\times 10^{-5}$)					Observed
Process	-2σ	-1σ	Median	$+1\sigma$	$+2\sigma$	($\times 10^{-5}$)
Br($Z \to \gamma\gamma$)	0.88	1.19	1.66	2.34	3.20	1.66
Br($Z \to \pi^0\gamma$)	1.21	1.63	2.28	3.21	4.37	2.28
Br($Z \to \pi^0\pi^0$)	0.93	1.23	1.72	2.41	3.29	1.73

TABLE V: 95% C.L. upper limits on the $Z \to \gamma\gamma$, $Z \to \pi^0\gamma$, and $Z \to \pi^0\pi^0$ branching ratios.

stringent Br(Z→$\gamma\gamma$) and Br(Z→$\pi^0\gamma$) limits were from LEP, which obtained a branching ratio limit on each signal of 5.2×10^{-5}. The CDF Br(Z→$\gamma\gamma$) and Br(Z→$\pi^0\gamma$) limits are, respectively, 3.1 and 2.3 times better that the LEP results. A Z→$\pi^0\pi^0$ branching ratio limit was not was not measured by the LEP experiment.

Using Equations 2–4 with the observed branching ratio limit, the number of signal events that we observe to exclude at 95% C.L. can be determined. The result is plotted with the background and data in Figure 7 for the signal region.

VII. CONCLUSIONS

We have presented a search for evidence of rare Z decays in the diphoton mass distribution using the full CDF data set, comprising 10.0 fb^{-1} of integrated luminosity. No such decays are observed in the data and we set 95% C.L. upper limits on the Z→$\gamma\gamma$, Z→$\pi^0\gamma$, and Z→$\pi^0\pi^0$ branching ratios. The expected branching ratio limit for the Z→$\gamma\gamma$, Z→$\pi^0\gamma$, and Z→$\pi^0\pi^0$ signals are 1.66×10^{-5}, 2.28×10^{-5}, and 1.72×10^{-5}, respectively. The observed branching ratio limits are 1.66×10^{-5}, 2.28×10^{-5}, and 1.73×10^{-5}, respectively. The CDF data produces limits on the Z→$\gamma\gamma$ and Z→$\pi^0\gamma$ branching ratios that are, respectively, 3.1 and 2.3 times better than the most stringent results from another experiment.

[1] L. D. Landau, Dokl. Akad. Nawk., USSR **60**, 207 (1948).
[2] C. N. Yang, Phys. Rev. **77**, 242 (1950).
[3] N. Kanda, R. Abe, T. Fujita, and H. Tsuda (2011), arXiv:1109.0926.
[4] J. Beringer et al. (Particle Data Group), Phys. Rev. D **86**, 010001 (2012).
[5] L. Amellos et al., Nucl. Phys. B **196**, 378 (1982).
[6] E. Glover et al. (1989), CERN report 89-08 Vol 2, G. Altarelli and C. Verzegnassi eds, (1989) 1.
[7] M. Acciarri et al., Phys. Lett. B **353**, 136 (1995).
[8] T. Aaltonen et al. (CDF Collaboration), Phys. Rev. Lett. **108**, 011801 (2012).
[9] T. Aaltonen et al. (CDF Collaboration), Physics Letters B **717**, 173 (2012).
[10] K. Bland (2011), FERMILAB-THESIS-2012-11.
[11] T. Sjostrand et al., Comput. Phys. Commun. **135**, 238 (2001), hep-ph/0010017.
[12] H. L. Lai et al. (CTEQ), Eur. Phys. J. **C12**, 375 (2000), hep-ph/9903282.
[13] R. Field and R. C. Group (CDF) (2005), hep-ph/0510198.
[14] T. Aaltonen et al. (CDF), Phys. Lett. B **692**, 232 (2010).
[15] D. Stump et al., JHEP **10**, 046 (2003), hep-ph/0303013.
[16] J. Pumplin et al., Phys. Rev. **D65**, 014013 (2002), hep-ph/0101032.
[17] P. M. Nadolsky and Z. Sullivan, eConf **C010630**, P510 (2001), hep-ph/0110378.
[18] D. Bourilkov, R. C. Group, and M. R. Whalley (2006), hep-ph/0605240.

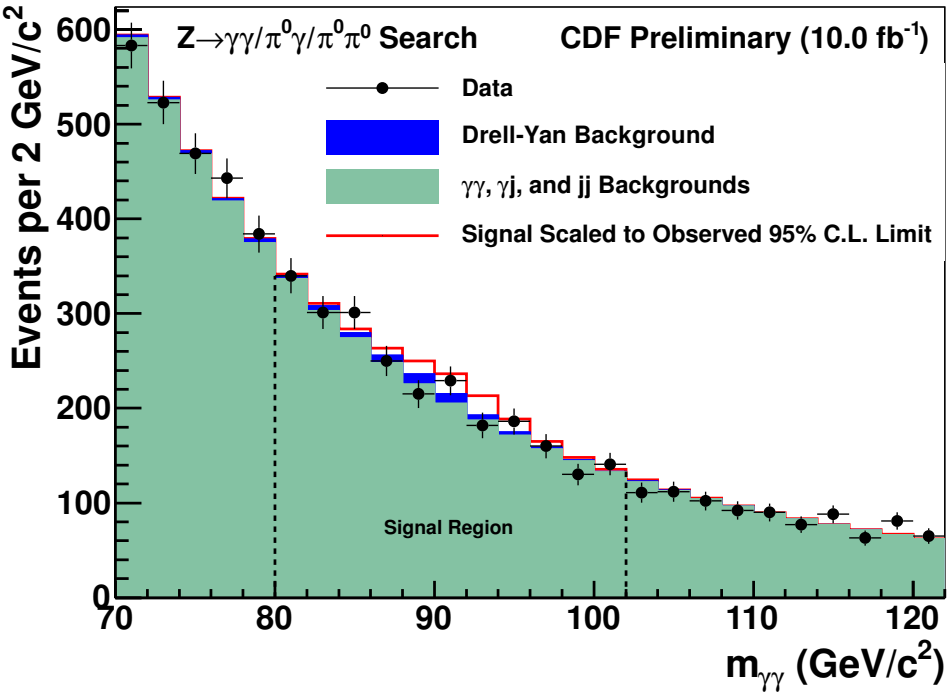

(a) Sideband plus signal region.

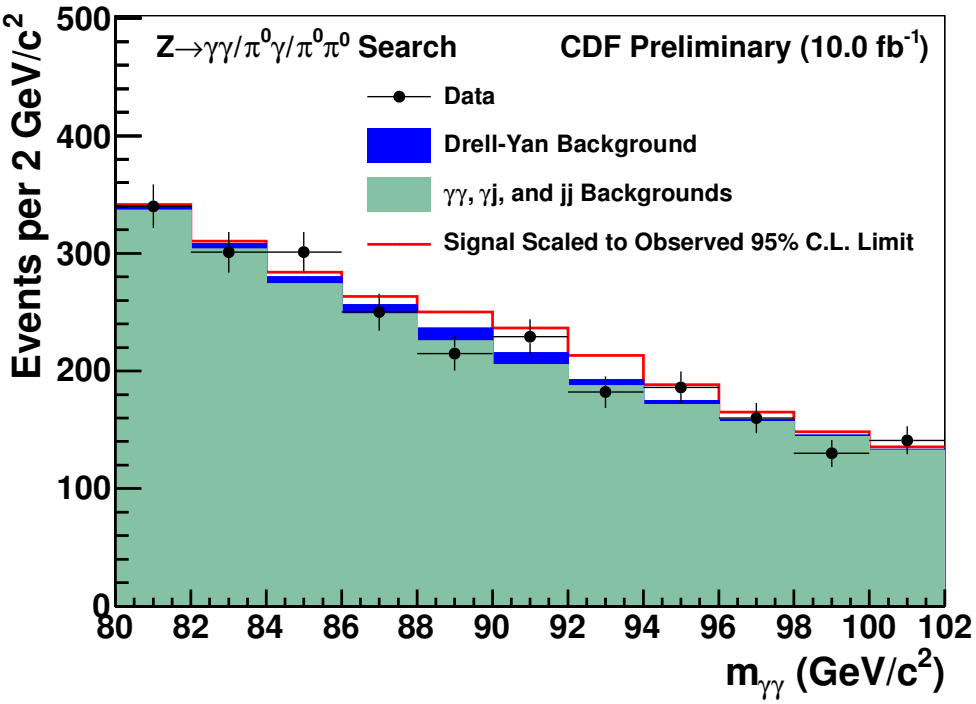

(b) Signal region.

FIG. 7: Background and data shown with an upper limit on the number of signal events that the CDF data excludes at 95% C.L.

Appendix A: Angular Distributions

In the helicity basis, we can write the expected angular distribution as

$$F(\alpha) = \sum_{m_Z \lambda_1 \lambda_2} f_{m_Z \lambda_1 \lambda_2} \left| d^{s_Z}_{m_Z \lambda_1 - \lambda_2}(\alpha) \right|^2 , \tag{A1}$$

where the sum is over independent polarization states of the initial particle (the Z boson) and over independent allowed helicity states of the decay products. The parameters/variables are defined as:

- α is the angle between the z axis and the momentum vector of the first decay product ($\vec{p_1}$), measured in the Z boson rest frame
- $s_Z = 1$ is the spin of the Z boson
- $m_Z = +1, 0, -1$ is the polarization of the Z boson, along the z axis
- λ_1 (λ_2) is the helicity of the first (second) decay product
- $f_{m_Z \lambda_1 \lambda_2}$ is the degree of polarization of a state
- $d^{s_Z}_{m_Z \lambda_1 - \lambda_2}(\alpha)$ a Wigner d function

Conservation of angular momentum places the following restriction:

$$|\lambda_1 - \lambda_2| \leq s_Z = 1 \tag{A2}$$

a. *Polarization of Generated Z bosons*

Since PYTHIA produces polarized Z boson states, we consider the three cases where the Z boson has a probability of f_+, f_0, and f_- of, respectively, being transversely polarized along the $+z$ axis, longitudinally polarized perpendicular to the z axis, and transversely polarized along the $-z$ axis. Due to symmetry, we have $f_- = f_+$.

b. *Angular Distribution of Z→$\nu_e\bar{\nu}_e$ Events*

With left-handed neutrinos (right-handed anti-neutrinos), the helicity is opposite (along) the direction of motion. This scenario yields possible combinations $|\lambda_1 - \lambda_2| = 1$ of $\frac{1}{2} - (-\frac{1}{2}) = 1$ and $-\frac{1}{2} - (\frac{1}{2}) = -1$. With $m_Z = +1, 0, -1$ and letting $\lambda_1 - \lambda_2 = 1$, we have three possible contributions to the net angular distribution:

$$\begin{aligned} F^{\nu\bar{\nu}}(\alpha) &= f_+ |d^1_{1,1}|^2 + f_0 |d^1_{0,1}|^2 + f_- |d^1_{-1,1}|^2 \\ &= f_+ |d^1_{1,1}|^2 + f_0 |d^1_{1,0}|^2 + f_- |d^1_{1,-1}|^2 \end{aligned} \tag{A3}$$

The states with $\lambda_1 - \lambda_2 = -1$ are the same and a factor of 2 can then be absorbed into the f_+, f_0, and f_- normalization parameters. This gives

$$\begin{aligned} F^{\nu\bar{\nu}}(\alpha) &= f_+ |1 + \cos\alpha|^2 + f_0 |\sin\alpha|^2 + f_+ |1 - \cos\alpha|^2 \\ &= f_+ (1 + \cos^2\alpha) + f_0 (1 - \cos^2\alpha) \\ &= (f_+ - f_0) \left(\frac{f_+ + f_0}{f_+ - f_0} + \cos^2\alpha \right) \end{aligned} \tag{A4}$$

where other constants are also absorbed into the normalization parameters. We obtain the values of f_+ and f_- by first writing

$$F^{\nu\bar{\nu}}(\alpha) = p_0 (p_1 + \cos^2\alpha) \tag{A5}$$

and then fitting the $\cos\alpha$ distribution for photons in the unweighted Z→$\gamma\gamma$ MC sample to this shape. The values $p_0 = 3708$ and $p_1 = 2810$ returned by the fit allow us to rewrite Eq. (A9) as

$$F^{\nu\bar{\nu}}(\alpha) = 2810 \left(1.32 + \cos^2\alpha \right) \tag{A6}$$

with $f_+ = 3259$ and $f_0 = 449$. This is the expected angular distribution for Z→$\nu_e\bar{\nu}_e$ events.

c. *Angular Distribution of Z→γγ Events*

The photons, being massless, have only transverse polarization states: $\lambda_{1,2} = \pm 1$. Along with this restriction, Eq. (A2) allows only the case where $\lambda_1 - \lambda_2 = 0$. We then have three possible contributions to the net angular distribution:

$$\begin{aligned} F^{\gamma\gamma}(\alpha) &= f_+|d^1_{1,0}|^2 + f_0|d^1_{0,0}|^2 + f_-|d^1_{-1,0}|^2 \\ &= f_+|d^1_{1,0}|^2 + f_0|d^1_{0,0}|^2 + f_-|d^1_{1,0}|^2 \end{aligned} \tag{A7}$$

This gives

$$\begin{aligned} F^{\gamma\gamma}(\alpha) &= f_+|\sin\alpha|^2 + f_0|\cos\alpha|^2 + f_+|\sin\alpha|^2 \\ &= f_+(1-\cos^2\alpha) + f_0(\cos^2\alpha) \\ &= (f_+ - f_0)\left(\frac{f_+}{f_+ - f_0} - \cos^2\alpha\right) \end{aligned} \tag{A8}$$

where constants are absorbed into the normalization parameters. Using the f_+ and f_0 values obtained in the previous section, we can write the expected photon angular distribution as

$$F^{\nu\bar{\nu}}(\alpha) = 2810\left(1.16 - \cos^2\alpha\right) \tag{A9}$$

We then obtain a $Z\to\nu_e\bar{\nu}_e$ to $Z\to\gamma\gamma$ reweighting function to correct the photon angular distribution for $Z\to\gamma\gamma$ events:

$$w_{\gamma\gamma}(\alpha) = \frac{F^{\gamma\gamma}(\alpha)}{F^{\nu_e\bar{\nu}_e}(\alpha)} = \frac{1.16 - \cos^2\alpha}{1.32 + \cos^2\alpha} \tag{A10}$$

d. *Angular Distribution of Z→π⁰γ Events*

For $Z\to\pi^0\gamma$ events, we have $\lambda_\gamma = 1$ or -1 and $\lambda_{\pi^0} = 0$. This gives $\lambda_\gamma - \lambda_{\pi^0} = \pm 1$, which are the same options that we had for $Z\to\nu_e\bar{\nu}_e$ decays. From this, we determine that the expected angular distribution for $Z\to\pi^0\gamma$ decays is the same as that for $Z\to\nu_e\bar{\nu}_e$ decays.

e. *Angular Distribution of Z→π⁰π⁰ Events*

For $Z\to\pi^0\pi^0$ events, we have $\lambda_{\pi^0} = 0$. This gives $\lambda_{\pi^0} - \lambda_{\pi^0} = 0$, which is the same option that we had for $Z\to\gamma\gamma$ decays. From this, we determine that the expected angular distribution for $Z\to\pi^0\pi^0$ decays is the same as that for $Z\to\gamma\gamma$ decays.